MODELLING OF SOLIDIFICATION OF ATOMISED DROPLETS

Romulo Heringer
LPT DFis CCE, Universidade Federal do Espírito Santo. 29075-514 Vitória ES, Brazil
romulo.heringer@lycos.com

Charles-André Gandin
CEMEF UMR CNRS-ENSMP 7635, Ecole des Mines de Paris, 06904 Sophia Antipolis, France
Charles-Andre.Gandin@ensmp.fr

Gérard Lesoult
LSG2M UMR CNRS-INPL-UHP 7584, Ecole des Mines de Nancy, 54042 Nancy, France
Gerard.Lesoult@mines.inpl-nancy.fr

Hani Henein
AMPL, University of Alberta, T6G 2G6 Edmonton, Canada
hani.henein@ualberta.ca

Abstract. In this work we present results of local measurements of the species composition made on atomized Al-Cu droplets. This analysis shows a non-uniform distribution of alloy compounds in the observed sections of the droplets. A numerical model was proposed for the solidification of a spherical droplet subject to convection. The solidification starts with an imposed undercooling at the center of the droplet and progresses spherically towards its external surface. Volume average of the energy and solute balances was taken for each phase. The numerical solution of these equations allowed to evaluate the distributions of the enthalpy, temperature, phase fractions, and solute composition in the droplet. Results are presented for a droplet of Al 10 wt% Cu, 250 μm-diameter and nucleation undercooling of 30°C. The model predicts the solute segregation in the droplet. It predicts also a systematic remelting of the supersaturated solid structures, which can be related with fragmentation and possible grain refining.

Keywords*: Solidification, numerical model, droplet, solute segregation, remelting*

1. Introduction

In the Impulse Atomization process, a plate separates the crucible from the atomizing chamber. The plate is perforated with cylindrical holes. Upon vibrations of the plate, the liquid is forced to flow through the holes and droplets of metal are formed in the atomizing chamber. The droplets then fall down and cool down simultaneously (Henein, 2002). At some undercooling of the melt, nucleation and fast propagation of a solid phase occurs.

In-situ measurement of the temperature history upon solidification is made difficult due to the size of the system and its rapid velocity during the fall. Modelling is thus particularly well suited for the study of droplet solidification formed by atomization. Heat flow modelling of a solidifying droplet is found in the literature with either a uniform temperature approximation (Prasad *et al.* 2002, Levi and Merahbian, 1982) or omission of the mushy zone Levi and Merahbian, 1982, Ajaev and Davis, 2003). A model has also been developed by Steinbach *et al.* (1999) in which the heat flow is solved in the liquid surrounding an envelope that represents the extent of the mushy zone. However, it considers a pure material with a constant mushy zone temperature equal to the melting point.

In the present contribution a numerical model based on diffusive flows is presented. The model predicts segregation taking place at the scale of an atomized droplet, thus extending the heat flow analysis previously proposed by Heringer *et al.* (2003). The full development of the present model can be found in Heringer (2004). The simulated composition profile resulting from the solidification of an Al - 10 wt% Cu is then compared with composition measurements performed by microprobe analysis.

2. Experimental

Impulse Atomization has been conducted in nitrogen on an Al - 10 wt% Cu melt (Henein, 2002, Prasad *et al.* 2002). Figure 1 presents the dendritic microstructure of a 250 μm-diameter droplet observed under a scanning electron microscope. The corresponding segregation map is shown in Figure 1. It is deduced from microprobe analyses: measurements with a 1 μm-diameter focused beam have been performed on a 4 μm-square grid. A large scatter of the composition map is found when simply drawing the 3204 collected data points. This behaviour was obviously expected since the focused beam hits either the core of a dendrite arm (in grey in Figure 1), a eutectic area (in white in Figure 1) or both. Consequently, in order to draw an average composition map over a representative volume of the microstructure, the following filter was applied: on each of the 3204 positions of the square grid, an average value of the composition is calculated by considering all measured values falling within a circle the centre of which corresponds to the square grid position. Little variation of the average composition map was found when changing the circle size within 20 μm to 40 μm-radius. Therefore, the value of 30 μm was kept as a reasonable value for the drawing of a meaningful segregation map.

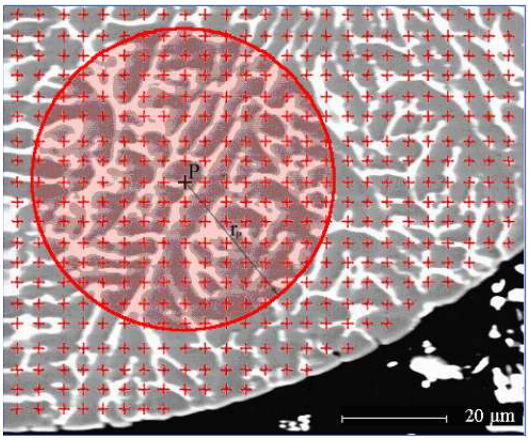

Figure 1. Schematics of the method defined to draw an average composition map from data points (superimposed crosses) using a focussed microprobe. Averaging disk diameter: 60 µm, square grid parameter: 4 µm.

3. Modelling

3.1. Macroscopic heat and solute flows

The model is based on a solution of the conservation equations for energy and mass fraction of solute written for a representative elementary volume (REV) made of a two-phase mixture. The assumptions related to the geometry and the transport phenomena are illustrated in Figure 2 and states as follows: h1) Approximate description of the dendritic mushy zone by average volume fractions of the solid and liquid phases, respectively g^s and g^l (with $g^s + g^l = 1$); h2) Droplet geometry simplified by a spherical domain of radius R; h3) Pure diffusive flows for both heat and solute; h4) No diffusion in the solid phase; h5) One-dimensional spherical heat and solute flows along $r \in [0, R]$.

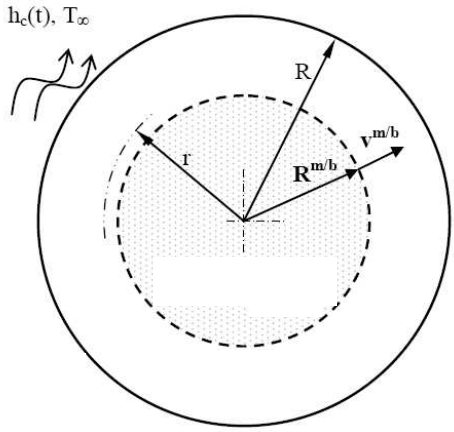

Figure 2. Schematics of the one-dimensional spherical mushy zone solidification model.

According to the above assumptions, the conservation equations can be written as follows:

$$\frac{\partial \langle H \rangle}{\partial t} = \frac{1}{r^2}\frac{\partial}{\partial r}\left[\langle k \rangle r^2 \frac{\partial T}{\partial r} \right], \quad (1)$$

$$\frac{\partial \langle w \rangle}{\partial t} = \frac{1}{r^2}\frac{\partial}{\partial r}\left[(1-g^s) D^l r^2 \frac{\partial \langle w^l \rangle^l}{\partial r} \right], \quad (2)$$

with:

$$\langle H \rangle = \langle C_p \rangle T + (1-g^s) L, \quad (3)$$

$$\langle w \rangle = g^s \langle w^s \rangle^s + (1-g^s) \langle w^l \rangle^l, \quad (4)$$

where $\langle H \rangle$ is the average volumetric enthalpy, T is the temperature, L is the volumetric enthalpy of fusion and t is the time. The average composition of the two-phase mixture, $\langle w \rangle$, is a function of the average composition of the solid, $\langle w^s \rangle^s$, and the average composition of the liquid, $\langle w^l \rangle^l$. The thermal properties of a phase $\varphi \in [s, l]$ are the average volumetric heat capacity, $\langle C_p^\varphi \rangle$, and the average thermal conductivity, $\langle k^\varphi \rangle$. The corresponding average properties of the mushy zone, $\langle C_p \rangle$ and $\langle k \rangle$, are calculated with the relationships:

$$\langle C_p \rangle = g^s \langle C_p^s \rangle^s + (1-g^s) \langle C_p^l \rangle^l, \quad (5)$$

$$\langle k \rangle = g^s \langle k^s \rangle^s + (1-g^s) \langle k^l \rangle^l. \quad (6)$$

The diffusion coefficient of solute in the liquid, D^l, is calculated using a pre-exponential factor, D_0^l, and an activation energy, Q^l, entering the Arrhenius law:

$$D^l = D_0^l \exp\left(-\frac{Q^l}{\Re T}\right), \tag{7}$$

where $\Re$ is the molar gas constant. The volume fraction of solid, g^s, is a function of both the volume fraction of the mushy zone, g^m, and the internal volume fraction of solid located within the mushy zone, g^{sm}, all these variables being defined for a REV:

$$g^s = g^m g^{sm}. \tag{8}$$

3.2. Front tracking and growth velocity

The volume fraction of the mushy zone, g^m, is determined for each REV thanks to a front tracking technique. The following additional assumptions are made: h6) Nucleation of a single grain at the centre of the spherical domain at a given undercooling, ΔT_N; h7) Radial propagation of the mushy zone in the undercooled liquid defining the position of a spherical envelope, $R^{m/b}$ (Figure 2); h8) Rate of propagation of the mushy zone growth front, $v^{m/b}$, given by a dendrite tip kinetics (Figure 2).

An envelope is defined between the spherical mushy zone and the surrounding extradendritic undercooled liquid in which it propagates that corresponds to the position of the dendrite tips, $R^{m/b}$. With the geometrical approximations used in assumptions h2, h5, h6 and h7, the volume fraction of the mushy zone is then a direct function of the position of the growth front and of the geometry of the REV:

$$g^m = f(R^{m/b}). \tag{9}$$

The position of the growth front is deduced from the integration over time of the growth velocity of the dendrite tips, $v^{m/b}$, from the time of the nucleation event, t_N:

$$R^{m/b} = \int_{t_N}^{t} v^{m/b}(t)\, dt \ . \tag{10}$$

A differential form of equation (10) is used for the numerical integration. The velocity of the growth front is calculated as a function of its temperature, $T^{m/b}$, using the following relationship:

$$v^{m/b} = A \left(T_L - T^{m/b}\right)^n, \tag{11}$$

$$T^{m/b} = T, \tag{12}$$

where A and n are constants determined by a fit of the velocity-temperature curve deduced from a dendrite tip kinetics model (Kurz *et al.* 1986) for the alloy of nominal composition, w_0. In the later model only the solutal and curvature contributions have been accounted for.

3.3. Mushy zone propagation

According to the approximation h4, the average composition of the solid phase, $\langle w^s \rangle^s$, is related to the internal volume fraction of solid located in the mushy zone, g^{sm}, via the relationship:

$$\frac{d}{dt}\left[g^{sm} \langle w^s \rangle^s\right] = w^{s/d} \frac{dg^{sm}}{dt}, \tag{13a}$$

where $w^{s/d}$ is the composition in the solid at the solid/liquid interface in the mushy zone, (s/d), where (d) denotes the interdendritic liquid located in the mushy zone (Figure 2).

The following additional assumptions are considered: h9) Uniform composition of the liquid in the mushy zone, $\langle w^d \rangle^d$; h10) Local equilibrium in the mushy zone at the solid/liquid interface (s/d) ***during solidification***: for an increase of the volume fraction of solid, the compositions at the solid/liquid interface in the solid, $w^{s/d}$, and in the liquid, $w^{d/s}$, are given by the phase diagram at the local temperature of the REV, T; h11) Linear approximations of the binary phase diagram for the liquidus and solidus monovariant lines, respectively T_L and T_S.

According to the above assumptions, one can write:

$$\langle w^d \rangle^d = w^{d/s}, \tag{14}$$

$$w^{d/s} = w_L, \tag{15}$$

$$w^{s/d} = w_S, \tag{16}$$

$$T_L = T_M + m_L\, w_L, \tag{17}$$

$$T_S = T_M + m_S\, w_S, \tag{18}$$

$$T_L = T, \tag{19}$$

$$T_S = T. \tag{20}$$

In the above equations (17) and (18), T_M is the melting temperature for pure aluminium, m_L and m_S are the constant slopes of the liquidus and solidus temperature and w_L and w_S are the compositions of the liquid and solid phases read on the x-axis coordinate of the phase diagram. The liquid of a volume that contains the mushy zone growth front, (l), is made of the extradendritic liquid, (b), and the interdendritic liquid, (d). The balance of the average liquid composition over the volume then writes:

$$(1-g^m g^{sm}) \langle w \rangle^l = g^m (1-g^{sm}) \langle w^d \rangle^d + (1-g^m) \langle w^b \rangle^b. \tag{21}$$

In order to determine the average composition in the melt located ahead of the growth front, $\langle w^b \rangle^b$, one more balance equation is written at the growth front (m/b):

$$\frac{\partial}{\partial t}\left[(1-g^m) \langle w^b \rangle^b\right] = \frac{1}{r^2}\frac{\partial}{\partial r}\left[(1-g^m)\, D^l\, r^2 \frac{\partial \langle w^b \rangle^b}{\partial r}\right] - \frac{A^{m/b}}{V^{REV}}\left(v^{m/b} \langle w^d \rangle^d - D^l \left.\frac{\partial w}{\partial r}\right|_{r=R^{b/m}}\right). \tag{22}$$

Details of the derivation of equation (22) can be found in Heringer (2004). Notations $A^{m/b}$ and V^{REV} represent the surface of the spherical mushy zone growth front and the volume of the REV, respectively.

The above set of twenty-two equations corresponds to a solution of the system made of twenty-two unknowns, including ten main unknowns ($\langle H\rangle$, $\langle w\rangle$, T, g^s, g^m, g^{sm}, $\langle w^l\rangle^l$, $\langle w^d\rangle^d$, $\langle w^b\rangle^b$, $\langle w^s\rangle^s$) and twelve second type unknowns ($\langle C_p\rangle$, $\langle k\rangle$, D^l, $R^{m/b}$, $v^{m/b}$, $T^{m/b}$, $w^{d/s}$, $w^{s/d}$, w_L, w_S, T_L, T_S).

3.4. Mushy zone solidification

When the mushy zone is fully developed in a given REV, i.e., $g^m = 1$, the solution does not require to track the growth of the mushy zone and several unknowns vanish ($R^{m/b}$, $v^{m/b}$, $T^{m/b}$, $\langle w^b\rangle^b$). As a consequence equations (9-12) and (22) are no longer used and equations (8) and (21) reduce to the simple forms, $g^s = g^{sm}$ and $\langle w^d\rangle^d = \langle w^l\rangle^l$, respectively. The system thus reduces to a solidification problem with fifteen unknowns, including six main unknowns ($\langle H\rangle$, $\langle w\rangle$, T, g^s, $\langle w^l\rangle^l$, $\langle w^s\rangle^s$) and nine second type unknowns ($\langle C_p\rangle$, $\langle k\rangle$, D^l, $w^{d/s}$, $w^{s/d}$, w_L, w_S, T_L, T_S).

3.5. Mushy zone remelting

During remelting of a fully developed mushy zone in a given REV, i.e., $g^m = 1$, while the composition of the interdendritic liquid, $\langle w^d\rangle^d$ (= $\langle w^l\rangle^l$), is still calculated using assumptions h9-h11 and thus applying Equations (14-15, 17, 19) (as for the case presented in section 3.4.), the average composition of the solid is interpolated over the composition profile $\langle w^s\rangle^s(g^s)$ stored during solidification. Thus, Equation (13a) is replaced by:

$$\langle w^s\rangle^s = \langle w^s\rangle^s(g^s). \tag{13b}$$

It should be outlined that such a treatment of remelting does not anymore require knowing the value of the solid composition at the solid/liquid interface, $w^{s/d}$. Equations (16, 18 and 20) and variables $w^{s/d}$, w_S and T_S are thus no longer unknowns of the system to solve.

3.6. Eutectic solidification

Upon reaching the eutectic temperature, a uniform temperature approximation is made up to completion of solidification. This is achieved by artificially blocking the temperature to the eutectic phase diagram temperature, T_E, and by converting an enthalpy variation into a variation of the fraction of solid. For the latter conversion, a derivative form of equation (3) is used.

3.7. Initial and boundary conditions, numerical implementation

Several additional assumptions are considered bellow: h12) A convective-type boundary condition is representative of the heat exchange with the external gas in which the droplet is atomized. Both the heat transfer coefficient, h_c, and the external temperature of the gas, T, are constant at the periphery of the droplet (r=R); h13) The metallic droplet does not exchange mass with the surrounding gas at the periphery of the droplet (r=R); h14) Adiabatic boundary conditions apply for both heat and mass transfers at the centre of the droplet (r=0); h15) Temperature, T_I, and composition fields, w_I, are uniforms within the liquid droplet at the beginning of the calculation (t=0).

The above boundary and initial conditions write:

$$\left.\frac{\partial T}{\partial r}\right|_{r=0} = 0, \tag{23}$$

$$-\langle k\rangle \left.\frac{\partial T}{\partial r}\right|_{r=R} = h_c\left(T(r=R,t) - T_\infty\right), \tag{24}$$

$$\left.\frac{\partial \langle w\rangle}{\partial r}\right|_{r=0} = 0, \tag{25}$$

$$\left.\frac{\partial \langle w\rangle}{\partial r}\right|_{r=R} = 0, \tag{26}$$

$$T(r, t=0) = T_I, \tag{27}$$

$$\langle w\rangle(r, t=0) = w_I. \tag{28}$$

Assumption (h6) is also written as an initial condition for nucleation:

$$T(r=0, t=t_N) < T_L - \Delta T_N, \tag{29}$$

where the unknown value is the nucleation time, t_N, when the temperature at the centre of the spherical liquid domain, r = 0, is sufficiently cooled down to reach the nucleation temperature, $T_L - \Delta T_N$. This time obviously depends on the temperature history at the centre of the domain and thus on the integration of the heat extraction rate through the surface of the droplet.

The finite volume method is used with a regular one-dimensional fixed mesh (Patankar, 1980). The time integration is based on a fully implicit scheme. Enthalpy is chosen as the main variable, while the temperature entering Equation (1) is replaced using a linear relationship $T = T^{\#} + [dT/d\langle H\rangle]^{\#}\left(\langle H\rangle - \langle H\rangle^{\#}\right)$, where symbol # refers to the last known value of the variable in an iterative procedure (M'Hamdi *et al.* 1999). Definition of the average volumetric enthalpy is used for the calculation of the linear relationship, leading to $dT/d\langle H\rangle = [\langle C_p\rangle - (dg^s/dT)\,L]^{-1}$. In fully liquid

and fully solid volumes, the later ratio simplifies to $dT/d\langle H\rangle = [C_p^{\varphi}]^{-1}$, with φ=[s, l]. In order to impose an isothermal transformation for the eutectic transformation, a sufficiently small value is fixed for the ratio $dT/d\langle H\rangle$ (e.g., $[10\ C_p^l]^{-1}$) until the volume is fully solid. Concerning Equation (2), the formulation proposed by Prakash and Voller (1989) has been implemented in order to calculate the average composition, $\langle w\rangle$. The three main steps of the iterative procedure consists of solving the heat flow equation assuming an initial value of $[dT/d\langle H\rangle]^{\#}$, the solute flow equation assuming an initial value of $[\langle w^l\rangle^l]^{\#}$, and then all other variables. Iterations are performed up to the convergence of both the temperature and the average composition fields.

4. Results

Figure 3b presents the result of the chemical analysis carried out on a 250 µm-diameter Al - 10 wt% Cu droplet. The local average composition is found to vary from 7 wt% to 12 wt%. No obvious direct correlation between the segregation map and the microstructure map is revealed. However, careful comparison between the phase fractions in Figure 3a and the distribution of Cu shows that the amount of eutectic (i.e., the local white area) is less where the average Cu content is low. Reproductions of these findings were made on several droplets (Heringer, 2004).

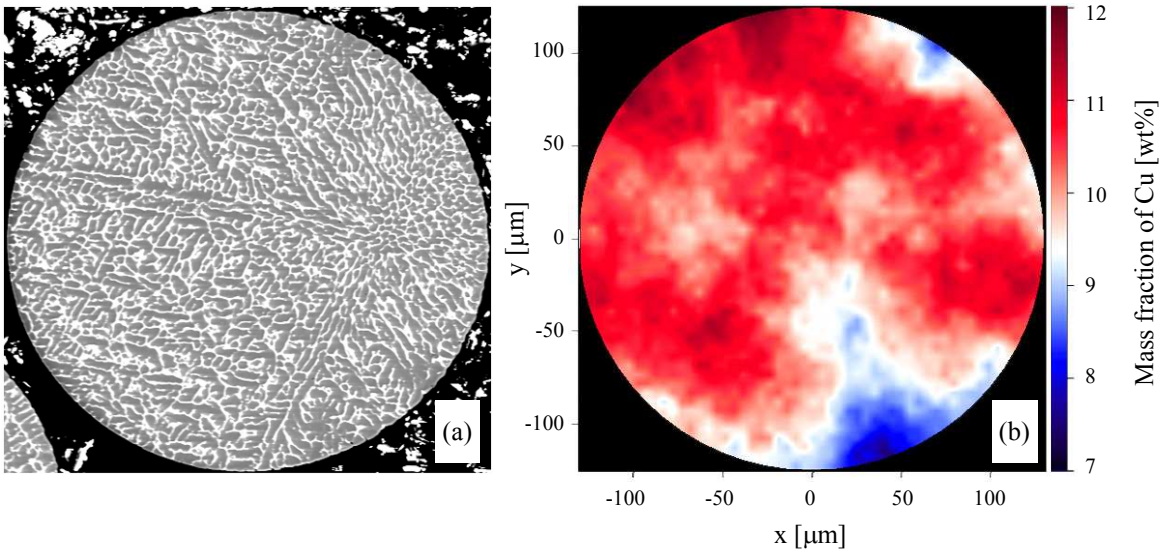

Figure 3. Cross-sections through the centre of a 250 µm-diameter Al - 10 wt% Cu droplet produced by atomization. (a) Dendritic microstructure observed in a scanning electron microscope and (b) corresponding average composition map deduced from microprobe analysis.

Table 1 Value of all parameters used in the calculations.

Symbol	Value	Symbol	Value	Symbol	Value
T_M	933.6 K	L	$9.5\cdot10^8$ J m^{-3}	n	2.7
m_L	-3.37 wt% K^{-1}	D_0^l	$1.05\cdot10^{-7}$ m^2 s^{-1}	h_c	490. W m^{-2} K^{-1}
m_S	-19.82 wt% K^{-1}	Q^l	23804. J mol^{-1}	T_∞	373. K
w_E	34.38 wt%	$\Re$	8.3145 J mol^{-1} K^{-1}	T_I (= T_L + 1)	900.9 K
w_0	10. wt%	κ^s	192.5 W m^{-1} K^{-1}	w_I (= w_0)	10. wt%
T_E	817.74 K	κ^l	100. W m^{-1} K^{-1}	ΔT_N	30. K
T_L	899.9 K	R	125.10^{-6} m	Mesh size	$3.125\cdot10^{-6}$ m
$C_p^s = C_p^l$	$3.\cdot10^6$ J m^{-3} K^{-1}	A	$3.57\cdot10^{-6}$ m s^{-1} K^{-n}	Time steps	10^{-5}-10^{-6} s

Table 1 summarizes the values of material properties and parameters used for the calculations. The value of the heat transfer coefficient, hc, was estimated using the model developed by Wiskel et al. (2002) for a value of the gas temperature typical of the impulse atomization process. A 30 K undercooling was chosen for the onset of results presented here. Initial temperature, T_I, was fixed one degree above the liquidus temperature and the initial composition, w_I, was taken equal to the nominal composition of the alloy, w_0.

Time evolutions of T computed at the centre, at mid-radius and at the periphery of the spherical domain are drawn in Figure 5a. The corresponding temperature profiles within the droplet at several times are shown in Figure 5a. These figures should be analysed simultaneously in order to explain the overall dynamic of the solidification. It is clearly shown that, as soon as nucleation takes place at the centre of the droplet (i.e., t_N = 0.016 s, r = 0), a temperature increase of the mushy zone is predicted. It rapidly reheats the whole system. Such reheating is due to the enthalpy of fusion

released by the growing mushy zone, which is not counterbalanced by the heat flux imposed at the surface of the droplet. In figure 5, the position of the growth front is directly made visible by the profile break down: an almost uniform temperature is found in the mushy zone, whereas a negative temperature gradient ahead of the growth front is predicted. This observation is confirmed by the superimposed temperature at the growth front, $T^{m/b}$, since it coincides with the position of the break down.

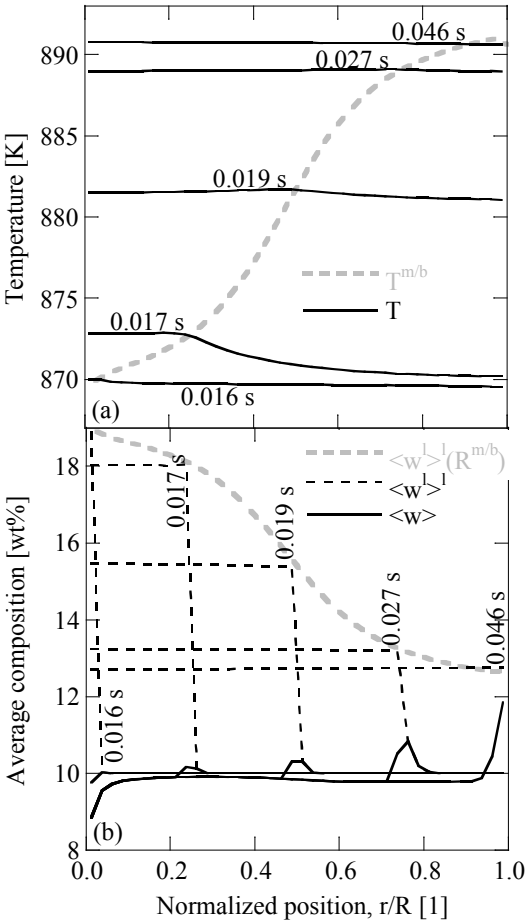

Figure 4. Predicted profiles of (a) the temperature, T, and (b) the average compositions, $\langle w \rangle$ and the average composition in the liquid, $\langle w^l \rangle^l$. The evolutions of the temperature and the average composition of the liquid tracked at the position of the growth front are also drawn, i.e. $T^{m/b}$ and $\langle w^l \rangle^l (R^{m/b})$, respectively.

The time evolution of the enthalpy and volume fraction of solid are presented in Figures 5b and 5c at the centre (r/R=0), mid-radius (r/R=0.5) and at the periphery of the droplet (r/R=1). It can be seen that the rapid growth of the mushy zone is accompanied by a sudden decrease of the enthalpy. This is explained by the corresponding sudden increase of the volume fraction of solid. The local reheating of the mushy zone during its propagation (Figure5a) results in a local decrease of the volume fraction of solid (Figure 5c), while the average volumetric enthalpy increases (Figure 5b). Only the volume located at the periphery of the droplet does not experience remelting (r/R=1). However, due to solute diffusion in the inter- and extra-dendritic liquid regions, the average composition of the droplet varies from 9 wt% at the centre to 12 wt% at the periphery. In order to explain the built-up of the macrosegregation, one can consider the composition profiles drawn in Figure 5b at several times. While a solute layer forms in the liquid ahead of the growth front, the average composition in the mushy zone is lower than the nominal composition. It remains almost constant during subsequent remelting/solidification.

The composition and enthalpy paths versus temperature are drawn in Figure 5d and 5e, respectively. The corresponding solidification paths are reported in Figure 5f. The liquidus, solidus and solvus lines, as well as the eutectic transformation, are added in Figure 5d. The typical sequences of the phase transformations are highlighted by letters for the mid-radius position: A→B *Cooling of the liquid* ($d\langle H \rangle/dt<0$, $dT/dt<0$, $g^s=0$, $g^m=0$, $\langle w \rangle=w_0$); B→C *Heating of the liquid* ($d\langle H \rangle/dt>0$, $dT/dt>0$, $g^s=0$, $g^m=0$, $d\langle w \rangle/dt>0$) - Negative gradients of composition and temperature exist in the liquid ahead of the mushy zone growth front; C→D *Mushy zone propagation* ($d\langle H \rangle/dt<0$, $dg^s/dt>0$, $dg^m/dt>0$, $d\langle w \rangle/dt<0$, $d\langle w^s \rangle^s/dt>0$) - Propagation of the mushy zone, with a volume fraction, g^m, going from 0 to 1. Heating is typical for larger nucleation undercooling, accompanied by an abrupt decrease of the enthalpy and an abrupt increase of

the volume fraction of solid. Solute leaves the mushy zone due to the negative composition gradient in the liquid ahead the growth front (Figure 5b); D→E *Mushy zone remelting* ($d\langle H\rangle/dt>0$, $dT/dt>0$, $dg^s/dt<0$, $g^m=1$, $d\langle w\rangle/dt=0$, $d\langle w^s\rangle^s/dt<0$) - During the increase of the temperature due to the reheating of the whole mushy zone, the volume fraction of solid decreases while the enthalpy increases; E→F *Mushy zone solidification* ($d\langle H\rangle/dt<0$, $dT/dt<0$, $dg^s/dt>0$, $g^m=1$, $d\langle w\rangle/dt=0$, $d\langle w^s\rangle^s/dt>0$); F→G *Eutectic solidification* ($d\langle H\rangle/dt<0$, $T=T_E$, $dg^s/dt>0$, $g^m=1$, $d\langle w\rangle/dt=0$, $d\langle w^s\rangle^s/dt>0$); G→H *Cooling of the solid* ($d\langle H\rangle/dt<0$, $dT/dt<0$, $g^s=1$, $g^m=1$, $d\langle w\rangle/dt=0$, $d\langle w^s\rangle^s/dt=0$)

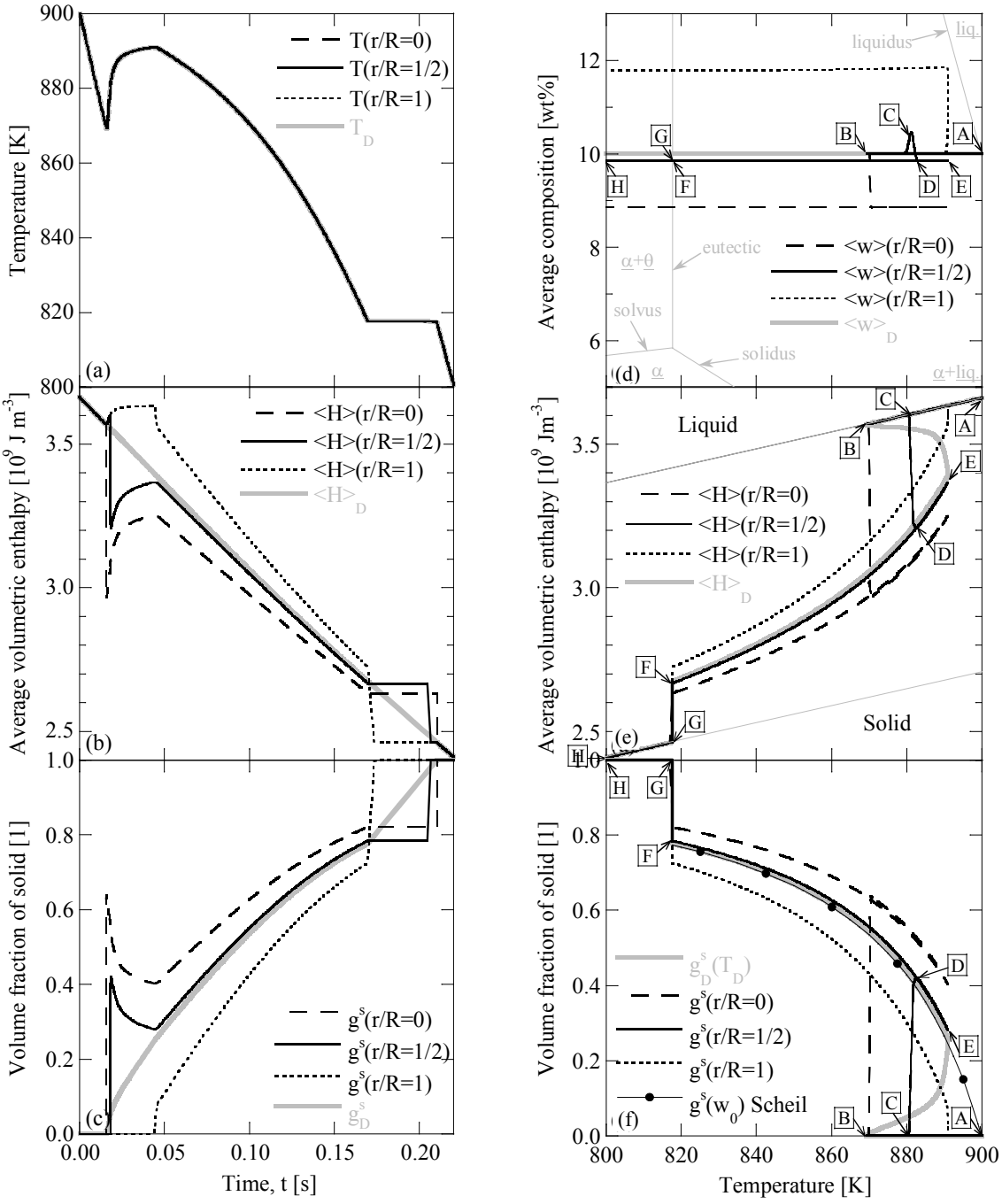

Figure 5. Predictions at the centre, r/R=0, at mid-radius, r/R=1/2, and at the periphery, r/R=1, of a spherical droplet of radius R. Left: Time evolutions of (c) T, (d) $\langle H\rangle$, and (e) g^s. Right: Predicted (a) $\langle H\rangle$, (b) $\langle w\rangle$, and (c) g^s, as a function of the temperature. Evolutions of the ariables averaged over the entire volume of the droplet, $\langle H\rangle_D$, $\langle w\rangle_D$ and g^s_D are also drawn as a function of the average droplet temperature, T_D.

4. Discussion

The integration of the enthalpy profile over the entire droplet is performed for the calculation of the average volumetric enthalpy of the droplet, $\langle H\rangle_D$. The same procedure is performed with the profile of the volume fraction of

solid, defining the average volume fraction of solid in the droplet, g^s_D. The latter two quantities are used to define an average droplet temperature, T_D, by using the following heat balance: $\langle H\rangle_D = \langle C\rangle_{p,D}\, T_D + (1-g^s_D)\, L$ where $\langle C\rangle_{p,D}$ is the heat capacity per unit volume whose value is chosen constant and equal in the solid and liquid phases (Table 1). Figure 5 presents the evolution of these average volumetric quantities as plain grey curves. Figure 5b and c present very simplified evolution of $\langle H\rangle_D$ and g^s_D. The average volumetric enthalpy of the droplet decreases almost linearly with time. This is due to the fact that an almost constant heat extraction rate, (h_c [T(r=R,t) - T_∞] 3/R), is found in the temperature interval considered and for $T(r=R,t) >> T_\infty$. The average volume fraction of solid of the droplet continuously increases as shown in Figure 5c. Since some heating is obviously retrieved on the average droplet temperature curve in Figure 5a, the occurrence of a recalescence at the scale of the droplet can be concluded ($d\langle H\rangle_D/dt<0$, $dT_D/dt>0$, $dg^s_D/dt>0$). However, from drawing these average quantities, the occurrence of remelting can not be concluded.

The model has been used in order to quantify the remelting and its distribution within the developing mushy zone. The time duration of the decrease of the local volume fraction of solid in Figure 5c corresponds to remelting. Remelting is enhanced when increasing the nucleation undercooling. An increase of the nucleation undercooling yet corresponds to a smaller remelting time (Heringer, 2004). It is also clearly shown that remelting does occur preferably close to the location of the nucleation event, i.e. close to the centre of the spherical domain. These observations are related to the recalescence taking place immediately after nucleation. Remelting takes place even if nucleation occurs at the liquidus temperature. Fragmentation is suggested as a possible mechanism to take into account in order to explain grain refining in droplets solidified from high undercooled melts (Karma, 1998). The mechanism would be that, upon the propagation of the dendritic network forming the grains, local remelting and break-off of dendrite arms take place. These dendrite arms are then transported, probably due to convection and sedimentation. It is to be noticed that a model has been proposed and validated that predicts fragmentation in undercooled liquid droplet (Karma, 1998). The author compares a time required for fragmentation to take place with the duration of a temperature plateau recorded during solidification experiments of levitated droplets. The present model could be useful for a better comprehension of the fragmentation and grain refining. Further discussion about this aspect of the present model can be found in Heringer (2004).

5. Conclusions

According to the model presented above, the main explanation for the macrosegregation map and the eutectic distribution observed in a particle of powder produced by atomization is the diffusion of solute in the liquid phase. Local remelting also play a role in the phase distribution, and consequently, in the macrosegregation map. The difference between recalescence ($d\langle H\rangle/dt<0$, $dT/dt>0$, $dg^s/dt>0$) and remelting ($d\langle H\rangle/dt>0$, $dT/dt>0$, $dg^s/dt<0$) is well identified with the model. It leads to the conclusion that recalescence occurs as a result of the propagation of the mushy zone in a given volume. Isothermal models considering the volume of the entire domain as the reference volume (Wang and Beckermann, 1993, Martorano et al. 2003), the recalescence stage is defined during the propagation of the mushy zone from the centre to the periphery of the grain. With the present non-isothermal model, recalescence is localized at the growth front while remelting takes place in the already existing mushy zone. This difference makes interpretation of remelting more consistent when considering the simultaneous evolutions of the local variables.

5. References

Ajaev, V. S. Davis, S. H. Journal of Computational Physics 2003, 187, 492.

Henein, H. Materials Science and Engineering. **326** (2002) 92-100.

Heringer, R. Gandin, Ch.-A. Lesoult, G. in Modeling of Casting, Welding and Advanced Solidification Processes X (Ed.: D. M. Stefanescu, J. A. Warren, M. R. Jolly, M. J. M. Krane), TMS, Warrendale, PA, USA, 2003, p. 549.

Heringer, R. Ph. D. Thesis, Institut National Polytechnique de Lorraine, Nancy (2004).(in french).

Karma, A. International Journal of Non-Equilibrium Processing **11** (1998) 201.

Kurz, W. Fisher, D. J. Fundamentals of Solidification, Trans Tech Pub., Aedermannsdorf, CH, 1998.

Kurz, W. Giovanola, B. Trivedi, R. Acta Metallurgica. **34** (1986) 823.

Levi, C. G. Mehrabian, R. Metallurgical Transactions A **13** (1982) 221.

Martorano, M. A. Beckermann, C. Gandin, Ch.-A. Metall. mater. trans. **34A** (2003) 1657-1674.

M'Hamdi, M. Combeau, H. Lesoult, G. Int. J. of Numerical Methods for Heat & Fluid Flow **9** (1999) 296.

Patankar, S. V. Numerical Heat Transfer and Fluid Flow, Hemisphere Pub. Co., NY, 1980.

Prakash, C. and Voller, V. Numerical Heat Transfer 1989, 15B, 171.

Prasad, A. Henein, H. Gandin, Ch.-A. Light Metals 2002, Metallurgical Society, Montréal, CAN, 2002.

Steinbach, I. Beckermann, C. Kauerauf, B. Li, Q. Guo, J. Acta Materialia 1999, 47, 971.

Wang, C. Y. Beckermann, C. Materials Science and Engineering A171 (1993) 199-211.

Wang, C. Y. Beckermann, C. Metallurgical Transactions 25A (1994) 1081-1093.

Wiskel, J. B. Henein, H. Maire, E. Canadian Metallurgical Quarterly 2002, 41, 97.

6. Responsibility notice

The authors are the only responsible for the printed material included in this paper.